Geochemical Perspectives Letters

Mercury isotopes in North Pacific sediments reveal vegetation expansion in warm climates

Y. Qu[1], R. Sun[2*], S. Li[2], Y. Yang[2], R. Hu[3], X. Yang[1], J. Zheng[1], X. Chen[2], Q. Hong[1], Z. Cao[4], D. Shi[4], J. Chen[2], T. Chen[1*]

https://doi.org/10.7185/geochemlet.2534

Abstract

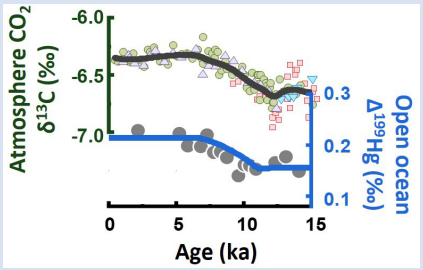

Mercury (Hg) concentrations and isotope compositions in sedimentary rocks are widely used to trace volcanism, but their natural variabilities through climate changes remain to be fully understood. Here, we present Hg isotope records from the North Pacific Shatsky Rise, a region without direct terrestrial input, to reconstruct the evolution of open ocean Hg isotopes. During the early Holocene (11–8 ka), the sedimentary Δ^{199}Hg increased from 0.16 ‰ to 0.21 ‰, along with the increase in δ^{13}C of CO_2 caused by the expansion of terrestrial vegetation. A higher Δ^{199}Hg (0.23 ‰) is also observed during the warm Pliocene (3.8–2.5 Ma) with higher terrestrial productivity. By constructing a time dependent global Hg box model, we demonstrate that the higher open ocean Δ^{199}Hg in warm climates reflects enhanced atmospheric Hg(0) uptake by terrestrial vegetation. This is likely driven by vegetation expansion and/or biome shifts, which absorb more gaseous Hg with lower Δ^{199}Hg.

Received 16 June 2025 | Accepted 28 July 2025 | Published 15 September 2025

Introduction

Sedimentary mercury (Hg) concentrations and isotope compositions are widely employed as volcanism proxies in palaeoenvironmental studies (Grasby *et al.*, 2019). The ratio of total mercury (THg) to total organic carbon (TOC) in sediments is suggested to reflect the changes in seawater Hg concentration and thus the atmospheric Hg load (Grasby *et al.*, 2019). Mercury isotopes exhibit both significant mass dependent (MDF) and mass independent fractionations (MIF) in natural systems, with the latter primarily generated through specific photochemical reactions (Blum *et al.*, 2014). Of particular interest, the odd MIF imparts negative Δ^{199}Hg values to atmosphere gaseous Hg(0) and positive values to oxidised Hg(II). Consequently, the terrestrial and open ocean Hg pools, sourced predominantly from atmospheric Hg(0) and Hg(II), exhibit negative and positive Δ^{199}Hg signatures, respectively (Jiskra *et al.*, 2021; Wang *et al.*, 2022).

Open ocean Hg burial is primarily driven by sinking particulate organic matter (POM) produced in the surface ocean. As POM sinks and degrades, the Hg bound to POC continuously exchanges with deep water through a process known as "regenerative scavenging" (Lamborg *et al.*, 2016). Since the inorganic Hg is the dominant Hg form in seawater (Bowman *et al.*, 2020), the Hg MIF preserved in open ocean sediments (mostly inorganic Hg) is interpreted to represent that of total Hg in the open ocean (Figueiredo *et al.*, 2022). Although the Hg-based proxies have been widely used in palaeoclimate research, the potential reorganisation of the global Hg cycle under different climate regimes remains to be constrained.

Here we present sedimentary records of open ocean Hg concentration and isotope compositions across contrasting climate states. The sediment records are recovered from Shatsky Rise in the North Pacific open ocean, a remote region far from the continental shelf and receiving minimal direct terrestrial input. A previous study indicates that its sedimentary organic matter is predominantly marine sourced (Maeda *et al.*, 2002). Dissolved Hg in the deep Northwest Pacific reflects both the deep water source signatures as well as the accumulation resulting from release during organic carbon remineralisation along the global ocean conveyer belt (Zhang *et al.*, 2014). Therefore, the Shatsky Rise sediment has the potential to provide valuable insights into global scale open ocean Hg cycling, while more records from other open ocean sites might help to assess regional variability in the future. Two climate periods without large scale volcanism are examined to assess the response of global Hg cycle to climate change, including the period since the Last Glacial Maximum (LGM, about 26 ka) and the warm Pliocene (3.8–2.5 Ma). The former reflects gradual warming and Earth system adjustments, while the latter represents the most recent period significantly warmer than the last glacial-interglacial cycle.

1. State Key Laboratory of Critical Earth Material Cycling and Mineral Deposits, School of Earth Sciences and Engineering, Nanjing University, Nanjing, 210023, China
2. Institute of Surface-Earth System Science, School of Earth System Science, Tianjin University, Tianjin, 300072, China
3. School of Geography and Ocean Science, Nanjing University, Nanjing, 210023, China
4. State Key Laboratory of Marine Environmental Science, College of Ocean and Earth Sciences, Xiamen University, Xiamen, 361102, China
* Corresponding author (email: ruoyu.sun@tju.edu.cn; tianyuchen@nju.edu.cn)

Materials and Methods

Sediment samples were recovered from Shatsky Rise in the North Pacific open ocean (36.13° N, 158.21° E, water depth of 3346 m). Gravity core KEC records the period since the LGM, whereas ODP Site 1208 archives the warm Pliocene period. Concentrations of total mercury and total organic carbon were determined, with relative standard deviations (RSD) less than 5 % and 2 %, respectively. The easily reducible Fe-Mn oxides are leached, which mainly represent authigenic Fe and Mn oxides in the Shatsky Rise sediment (Qu *et al.*, 2024). The Hg isotope compositions were measured in Tianjin University, with 2 s.d. uncertainty for δ^{202}Hg, Δ^{199}Hg and Δ^{200}Hg of 0.10 ‰, 0.05 ‰, and 0.04 ‰, respectively. To evaluate the response of the global Hg cycle to climate changes, we adapted a five-box model comprising atmospheric Hg(0) and Hg(II) reservoirs, a terrestrial reservoir, and a coastal and open ocean reservoir. Detailed information on samples, analytical protocols, and model configuration is provided in the Supplementary Information.

Results

In the record since the LGM, the TOC concentration is higher during the glacial period (26–11 ka) than the Holocene (11–0 ka) (Fig. 1). An increase in authigenic Fe and Mn oxide concentrations is observed during the Holocene, when THg exhibits large variations and the THg/TOC ratio increases (Fig. 1b,c). Compared to core KEC, the warm Pliocene record displays lower TOC and THg concentrations but a slightly higher and more variable THg/TOC ratio.

The Hg isotope data for core KEC and Site 1208 are shown in Figure 2. The δ^{202}Hg for core KEC has no long-term trend since the LGM (Fig. 2a). The Δ^{199}Hg rises during the early Holocene (11–8 ka), and is significantly higher in the mid- to late Holocene (8–0 ka; 0.21 ± 0.03 ‰, 2 s.d., n = 5) than in the glacial period (26–11 ka; 0.16 ± 0.06 ‰, 2 s.d., n = 14; unpaired Wilcoxon test, $p < 0.05$). For Site 1208, the δ^{202}Hg and Δ^{199}Hg exhibit no secular change. The average Δ^{199}Hg of Site 1208 samples for the Pliocene is 0.06 ‰ higher (unpaired Wilcoxon test, $p < 0.05$) than that of core KEC samples since the LGM (0.23 ‰ *vs.* 0.17 ‰) (Fig. 2g). The Δ^{200}Hg shows no secular change and has no systematical difference between core KEC and Site 1208 sediments. Details on Hg isotope data are provided in the Supplementary Information.

Discussion

Higher sedimentary Δ^{199}Hg during warm climate states. In the record since the LGM, the lower TOC and higher authigenic Fe and Mn oxides (Fig. 1) indicate lower productivity and higher bottom water oxygenation during Holocene than the glacial period (Maeda *et al.*, 2002; Galbraith *et al.*, 2007). In the oxic Holocene sediment, the THg/TOC ratio has a higher value and larger variability than the glacial period due to the early diagenetic effect (Qu *et al.*, 2024). Similar phenomenon in THg/TOC ratio is also observed in the warm Pliocene sediment (Fig. 1f) with high bottom water oxygenation (Abell and Winckler, 2023). The diagenetic mobilisation of Hg prohibits using THg/TOC and δ^{202}Hg to reliably record past seawater signatures. However, the sedimentary Δ^{199}Hg has been shown to be resistant to diagenesis, thus mostly retaining the seawater signal (Chen *et al.*, 2022).

The observed Δ^{199}Hg values in Shatsky Rise sediment are significantly higher than those reported for pre-anthropogenic marine sediments deposited along continental margins

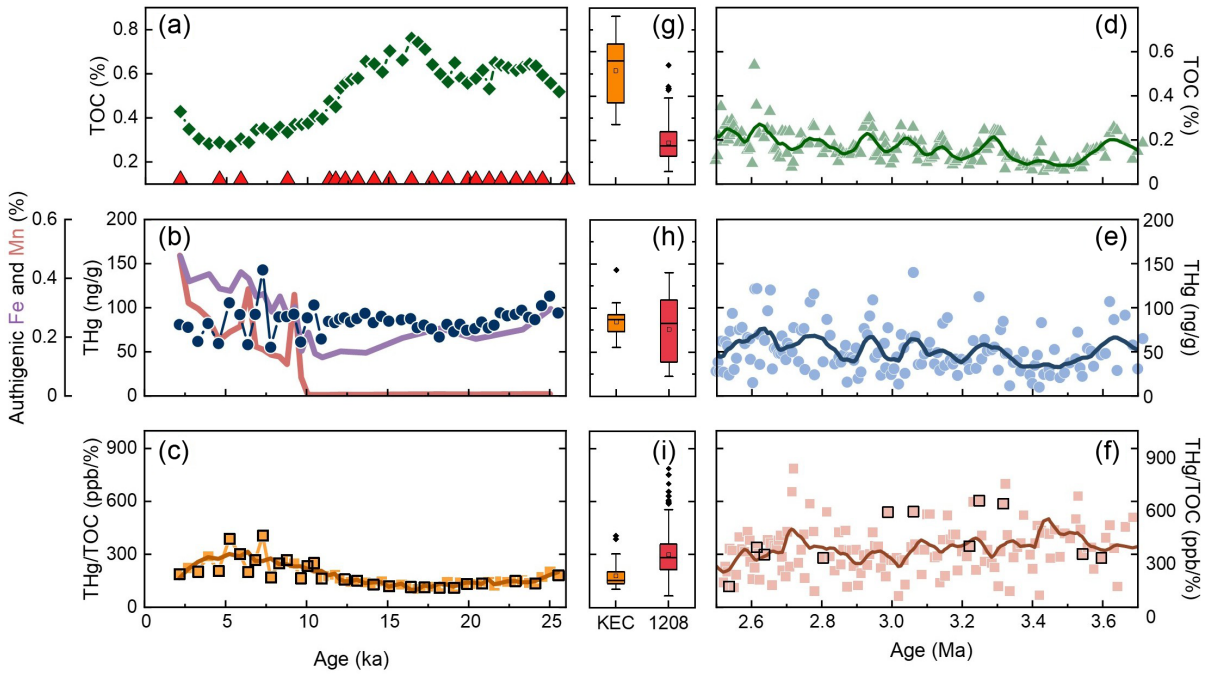

Figure 1 The geochemical data of the Shatsky Rise sediment. **(a–c)** The geochemical data of core KEC, including the TOC concentration, THg (blue circles) in comparison with authigenic Fe (purple) and Mn (red lines) concentration, and THg/TOC ratio. The red triangles in **(a)** indicate age control points by ^{14}C dating (see details in Supplementary Information). The bold brown line in **(c)** is the regression line of the 5-point LOESS smoothing of THg/TOC. **(d–f)** The geochemical data of Site 1208, including the TOC concentration, THg, and THg/TOC ratio. The bold lines in **(d–f)** are regression lines with 12-point LOESS smoothing. Squares outlined in black denote samples analysed for Hg isotopes. **(g–i)** Box-plots comparing the TOC, THg, THg/TOC data between core KEC and Site 1208.

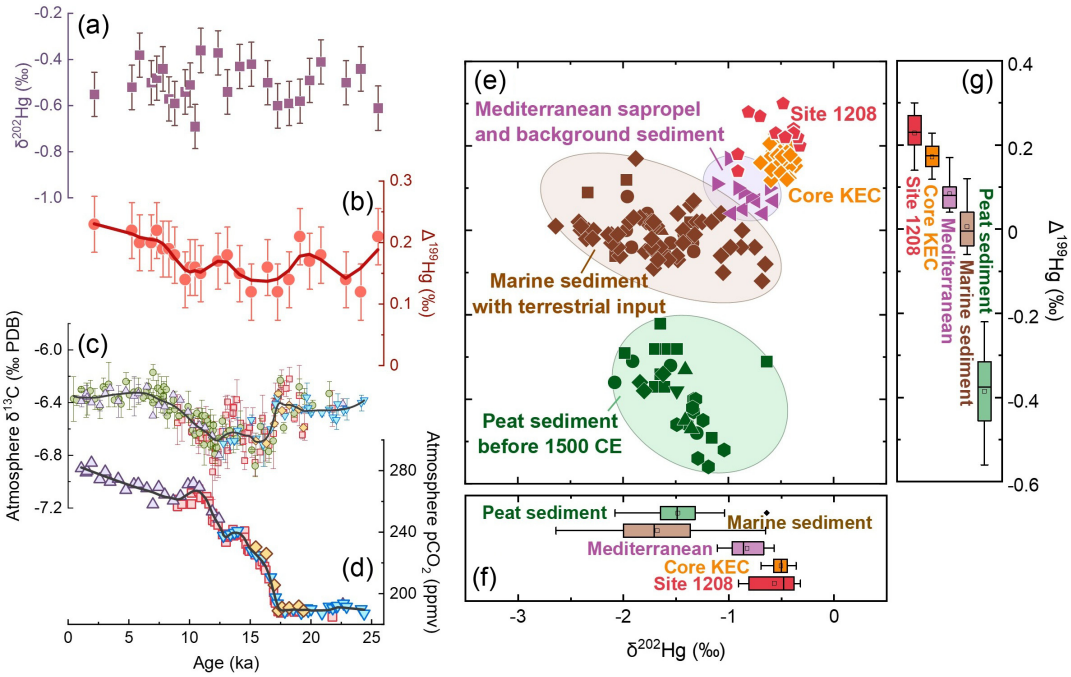

Figure 2 The Hg isotope data of the Shatsky Rise sediment. **(a,b)** The δ^{202}Hg and Δ^{199}Hg records. Error bars represent the 2 s.d. measurement uncertainty, which are 0.10 ‰ and 0.05 ‰ for δ^{202}Hg and Δ^{199}Hg, respectively. The dark red bold line is the regression line of 5-point LOESS smoothing of Δ^{199}Hg. **(c,d)** The atmosphere CO_2 concentration and $\delta^{13}C_{atm}$ recorded in ice cores (Schmitt *et al.*, 2012). The thick lines represent the weighted average across different sites and approaches as indicated by different symbols. **(e)** The Hg isotope data of this study are compared with a compilation of published pre-anthropogenic Hg data. The Hg isotope data of core KEC and Site 1208 are in orange and red, respectively. Brown symbols are samples from the Arctic Ocean (Gleason *et al.*, 2017) and the South Atlantic Ocean (Figueiredo *et al.*, 2022), which are known to receive direct terrestrial input. Purple symbols are Mediterranean sediments (Gehrke *et al.*, 2009). Peat sediments (Enrico *et al.*, 2017; Li *et al.*, 2023) deposited before 1500 AD are summarised as natural terrestrial Hg isotope endmember. **(f,g)** Box-plots comparing the dataset shown in **(e)**.

(Fig. 2e) (Gehrke *et al.*, 2009; Gleason *et al.*, 2017; Figueiredo *et al.*, 2022), suggesting little influence from terrestrial input of negative Δ^{199}Hg. Given its open ocean setting, the Shatsky Rise has the potential to provide an open ocean Δ^{199}Hg reference value, and most likely records the open ocean Δ^{199}Hg evolution through climate changes (see details in the Supplementary Information). The most prominent feature of the Δ^{199}Hg record since the LGM is the clear increasing trend during the early Holocene (~11 to 8 ka), which is similar to the rise in atmosphere CO_2 carbon isotope ($\delta^{13}C_{atm}$) (Fig. 2b,c). The deglacial atmospheric CO_2 (pCO_2) increase results in a warmer and wetter climate in the early Holocene, which promotes the expansion of terrestrial vegetation (Prentice *et al.*, 2011; Ciais *et al.*, 2012). The enhanced terrestrial productivity preferentially assimilates the lighter carbon isotope (^{12}C relative to ^{13}C) from the atmosphere and leads to the $\delta^{13}C_{atm}$ increase. The same process has been shown to increase terrestrial uptake of Hg(0) (Jiskra *et al.*, 2018), characterised by a negative Δ^{199}Hg value. Therefore, the increased terrestrial Hg fixation and burial would elevate the Δ^{199}Hg of the atmosphere and open ocean system considering the mass balance of Hg isotopes in the whole Earth surface system.

Water column processes, including methylmercury degradation and Hg(II) reduction, may also have an influence on the Δ^{199}Hg signature of the open ocean Hg and thus the sediment record. However, if these processes were the primary driver of sedimentary Δ^{199}Hg evolution, the record would be expected to follow the glacial-interglacial changes in environmental factors in the northwest Pacific (Rae *et al.*, 2020), such as solar radiation, dissolved oxygen, and productivity. The absence of a distinct Δ^{199}Hg shift during deglaciation, coupled with its co-variation with $\delta^{13}C_{atm}$ during the Holocene (11–0 ka) ($\rho = 0.85$, $p < 0.05$; Spearman's rank correlation analysis), suggests that water column processes are likely not the primary drivers. The Δ^{200}Hg *versus* Δ^{199}Hg relationship further supports limited net MIF in the water column, where the sedimentary data are mostly on the mixing line of atmospheric Hg(0) and Hg(II) sources (see details in the Supplementary Information). The open ocean Δ^{199}Hg signature is thus dictated by its major source, the atmospheric Hg(0) and Hg(II) deposition (Jiskra *et al.*, 2021), followed by transport to the deep ocean through deep water formation and POM remineralisation, and deposition in the sedimentary matter. Therefore, the increasing Δ^{199}Hg observed in Shatsky Rise sediments during the early Holocene can be well explained by elevated atmospheric Δ^{199}Hg due to enhanced terrestrial vegetation growth and associated Hg sequestration.

Another typical warm climate state is the Pliocene when there was limited Northern Hemisphere Glaciation (Fedorov *et al.*, 2013). The terrestrial vegetation was more productive and the arid areas such as deserts were smaller during the warm Pliocene when the Northern Hemisphere was covered by high-latitude forests rather than the modern tundra-type vegetation (Haywood and Valdes, 2006). The open ocean Δ^{199}Hg recorded by Shatsky Rise sediment is also higher (unpaired Wilcoxon test, $p < 0.05$) during the warm Pliocene ($\Delta^{199}Hg = 0.23 \pm 0.09$ ‰, 2 s.d., n = 11) than the period since the LGM ($\Delta^{199}Hg = 0.17 \pm 0.06$ ‰, 2 s.d., n = 25). The comparison of the two climate states reveals a consistently higher open ocean Δ^{199}Hg during warmer climates when terrestrial vegetation productivity is enhanced. In the following, we will use a time-dependent atmosphere-terrestrial-ocean box model to quantitatively explore the mechanism for the observed Δ^{199}Hg changes.

Modelling representation of natural Hg cycles. Using the simplified Hg isotope box model, we first test whether the observed Δ^{199}Hg shift could be explained by enhanced Hg(0) uptake by the terrestrial vegetation system. Given that atmospheric and oceanic circulation may experience adjustment during the early Holocene, other scenarios that could affect open ocean Δ^{199}Hg are also explored, including increased atmospheric Hg(II) deposition to the open ocean, decreased sedimental Hg burial efficiency in open ocean, and decreased coastal to open ocean connectivity due to sea level rising.

By using well constrained parameters (sizes of reservoirs, fluxes between reservoirs, and isotope fractionation factors of Δ^{199}Hg), the model is set as steady states during the late Holocene and the deglacial, and all perturbations in different simulation scenarios are introduced during the early Holocene. Modelling details are provided in the Supplementary Information. In the first scenario, the model prescribes that vegetation Hg(0) uptake contributes about 70 % of the terrestrial Hg fixation relative to about 30 % from atmospheric Hg(II) in the late Holocene, based on modern observations (Wang *et al.*, 2022). The atmospheric Hg(0) deposition flux into the vegetation before the early Holocene is set at a low value to account for the change in terrestrial biosphere since the early Holocene. The result suggests that enhanced terrestrial Hg(0) uptake flux by a factor of 1.7 relative to the deglacial steady state could broadly reproduce the observed Δ^{199}Hg shift during the early Holocene (Fig. 3a). This is consistent with previous studies of the $\delta^{13}C_{atm}$ record and modelling results, which suggest that the expansion of the terrestrial biosphere during the early Holocene (Schmitt *et al.*, 2012) increased the terrestrial primary productivity by a factor of 1.43 to 2.00 (Prentice *et al.*, 2011; Ciais *et al.*, 2012).

In the second and third scenarios, the increase in atmospheric Hg(II) deposition flux and the decreased Hg burial in the open ocean are considered during the early Holocene. To reproduce the observed Δ^{199}Hg shift, large variations in precipitation (2.4×) or POM-related open ocean Hg burial flux (0.6×) are needed during the early Holocene, which are not supported by previous studies (Cartapanis *et al.*, 2016; Hancock *et al.*, 2023). In the fourth scenario, Hg transport flux from the coastal to open ocean decreased by a factor of 0.33. However, the deglacial sea level rise and the associated decrease in coastal-open ocean connectivity starts at about 17.5 ka (Yokoyama *et al.*, 2018), predating the observed Δ^{199}Hg increase. The timing thus precludes the change in coastal to open ocean Hg transport as the prominent driver of open ocean Δ^{199}Hg shift. Based on the open ocean Δ^{199}Hg record and the four modelling scenarios, we suggest that the early Holocene Δ^{199}Hg increase is most probably caused by increased Hg(0) uptake by the terrestrial ecosystem.

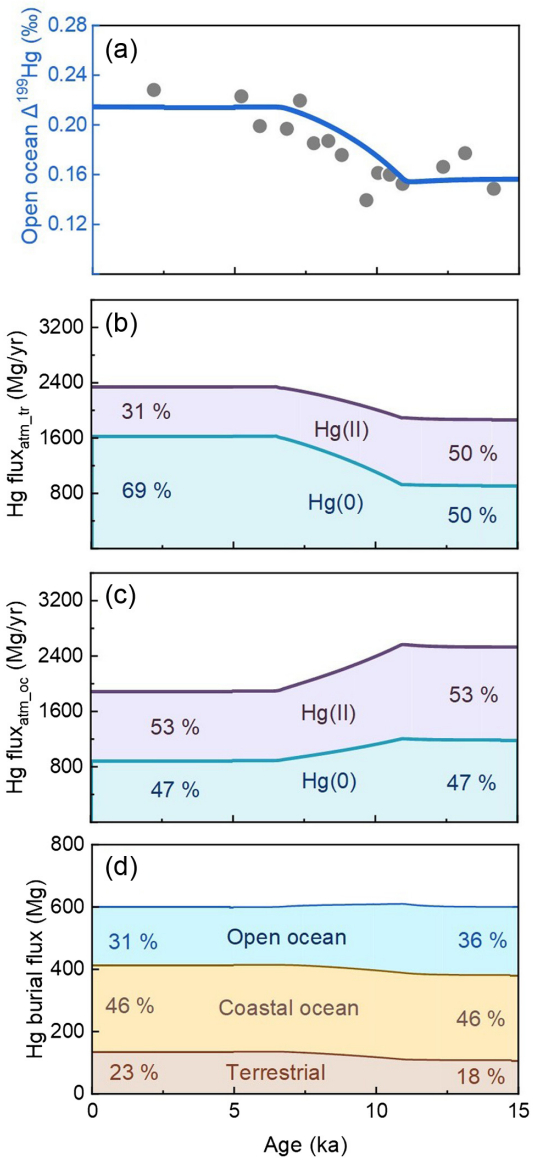

Figure 3 Modelling output illustrating the impact of enhanced atmospheric Hg(0) uptake by the terrestrial system during the early Holocene. **(a)** The observed (grey points) and model output (blue lines) of the open ocean Δ^{199}Hg. **(b)** The atmospheric Hg deposition flux to the terrestrial system, with the blue and purple shades indicating Hg(0) and Hg(II) deposition flux, respectively. The percentages indicate the relative contribution of Hg(0) and Hg(II). **(c)** The atmospheric Hg deposition flux to the open ocean. The shades and percentages are the same as the second row. **(d)** The Hg burial flux and burial ratio through terrestrial (brown), coastal (yellow), and open ocean (blue) systems.

Conclusions and Implications

The Hg isotope record from North Pacific open ocean sediments at the Shatsky Rise reveals elevated Δ^{199}Hg values during warm periods, including the mid- to late Holocene and the warm Pliocene. Using a simplified Hg isotope box model, we propose that the expansion of the terrestrial biosphere is likely the primary driver of this pattern, highlighting the significant role of terrestrial vegetation in the global Hg cycle. Previous research on modern atmospheric Hg(0) indicates that vegetation uptake of Hg(0) is a crucial factor in regulating Hg distribution between the atmosphere and terrestrial system on a seasonal timescale (Jiskra *et al.*, 2018). This work suggests that the vegetation uptake of Hg(0) might also be the dominant factor driving the global Hg cycle across various climate states on a longer timescale. In the context of global change, the responses of terrestrial Hg and carbon cycles remain unclear due to the intricate mechanisms governing terrestrial ecosystem responses (Luo, 2007). By showing enhanced terrestrial productivity and Hg and carbon stocks during past warm climate states, our study offers insights into potential future responses. With the forest ecosystem restoration (Watson *et al.*, 2018), the terrestrial biosphere has the potential to store more Hg from the atmosphere and thus alleviate Hg pollution in the open ocean. Additionally, our results highlight the need to consider significant climate and environmental adjustments when using Hg concentrations and isotopes to trace large scale volcanism in the geological history.

Acknowledgements

We are grateful to the editor and two reviewers for their constructive comments and suggestions. This research is funded by the National Key Research and Development Program of China (2023YFF0805004), and the National Natural Science Foundation of China (41991325, 42373011, 42173081, 42373011). This research used samples and data provided by Ocean Drilling Program (ODP). The KEC samples were collected onboard of R/V Tan Kah Kee implementing the open research cruise NORC2022-306 supported by NSFC Shiptime Sharing Project (project number: 42149303).

Editor: Gavin Foster

Additional Information

Supplementary Information accompanies this letter at https://www.geochemicalperspectivesletters.org/article2534.

Cite this letter as: Qu, Y., Sun, R., Li, S., Yang, Y., Hu, R., Yang, X., Zheng, J., Chen, X., Hong, Q., Cao, Z., Shi, D., Chen, J., Chen, T. (2025) Mercury isotopes in North Pacific sediments reveal vegetation expansion in warm climates. *Geochem. Persp. Let.* 36, 48–53. https://doi.org/10.7185/geochemlet.2534

References

Abell, J.T., Winckler, G. (2023) Long-Term Variability in Pliocene North Pacific Ocean Export Production and Its Implications for Ocean Circulation in a Warmer World. *AGU Advances* 4, e2022AV000853. https://doi.org/10.1029/2022AV000853

Blum, J.D., Sherman, L.S., Johnson, M.W. (2014) Mercury Isotopes in Earth and Environmental Sciences. *Annual Review of Earth and Planetary Sciences* 42, 249–269. https://doi.org/10.1146/annurev-earth-050212-124107

Bowman, K.L., Lamborg, C.H., Agather, A.M. (2020) A global perspective on mercury cycling in the ocean. *Science of the Total Environment* 710, 136166. https://doi.org/10.1016/j.scitotenv.2019.136166

Cartapanis, O., Bianchi, D., Jaccard, S.L., Galbraith, E.D. (2016) Global pulses of organic carbon burial in deep-sea sediments during glacial maxima. *Nature Communications* 7, 10796. https://doi.org/10.1038/ncomms10796

Chen, D., Ren, D., Deng, C., Tian, Z., Yin, R. (2022) Mercury loss and isotope fractionation during high-pressure and high-temperature processing of sediments: Implication for the behaviors of mercury during metamorphism. *Geochimica et Cosmochimica Acta* 334, 231–240. https://doi.org/10.1016/j.gca.2022.08.010

Ciais, P., Tagliabue, A., Cuntz, M., Bopp, L., Scholze, M., Hoffmann, G., Lourantou, A., Harrison, S.P., Prentice, I.C., Kelley, D.I., Koven, C., Piao, S.L. (2012) Large inert carbon pool in the terrestrial biosphere during the Last Glacial Maximum. *Nature Geoscience* 5, 74–79. https://doi.org/10.1038/ngeo1324

Enrico, M., Le Roux, G., Heimbürger, L.-E., Van Beek, P., Souhaut, M., Chmeleff, J., Sonke, J.E. (2017) Holocene Atmospheric Mercury Levels Reconstructed from Peat Bog Mercury Stable Isotopes. *Environmental Science & Technology* 51, 5899–5906. https://doi.org/10.1021/acs.est.6b05804

Fedorov, A.V., Brierley, C.M., Lawrence, K.T., Liu, Z., Dekens, P.S., Ravelo, A.C. (2013) Patterns and mechanisms of early Pliocene warmth. *Nature* 496, 43–49. https://doi.org/10.1038/nature12003

Figueiredo, T.S., Bergquist, B.A., Santos, T.P., Albuquerque, A.L.S., Silva-Filho, E.V. (2022) Relationship between glacial CO_2 drawdown and mercury cycling in the western South Atlantic: An isotopic insight. *Geology* 50, 801–805. https://doi.org/10.1130/G49942.1

Galbraith, E.D., Jaccard, S.L., Pedersen, T.F., Sigman, D.M., Haug, G.H., Cook, M., Southon, J.R., Francois, R. (2007) Carbon dioxide release from the North Pacific abyss during the last deglaciation. *Nature* 449, 890–893. https://doi.org/10.1038/nature06227

Gehrke, G.E., Blum, J.D., Meyers, P.A. (2009) The geochemical behavior and isotopic composition of Hg in a mid-Pleistocene western Mediterranean sapropel. *Geochimica et Cosmochimica Acta* 73, 1651–1665. https://doi.org/10.1016/j.gca.2008.12.012

Gleason, J.D., Blum, J.D., Moore, T.C., Polyak, L., Jakobsson, M., Meyers, P.A., Biswas, A. (2017) Sources and cycling of mercury in the paleo Arctic Ocean from Hg stable isotope variations in Eocene and Quaternary sediments. *Geochimica et Cosmochimica Acta* 197, 245–262. https://doi.org/10.1016/j.gca.2016.10.033

Grasby, S.E., Them, T.R., Chen, Z., Yin, R., Ardakani, O.H. (2019) Mercury as a proxy for volcanic emissions in the geologic record. *Earth-Science Reviews* 196, 102880. https://doi.org/10.1016/j.earscirev.2019.102880

Hancock, C.L., McKay, N.P., Erb, M.P., Kaufman, D.S., Routson, C.R., Ivanovic, R.F., Gregoire, L.J., Valdes, P. (2023) Global Synthesis of Regional Holocene Hydroclimate Variability Using Proxy and Model Data. *Paleoceanography and Paleoclimatology* 38, e2022PA004597. https://doi.org/10.1029/2022PA004597

Haywood, A.M., Valdes, P.J. (2006) Vegetation cover in a warmer world simulated using a dynamic global vegetation model for the Mid-Pliocene. *Palaeogeography, Palaeoclimatology, Palaeoecology* 237, 412–427. https://doi.org/10.1016/j.palaeo.2005.12.012

Jiskra, M., Sonke, J.E., Obrist, D., Bieser, J., Ebinghaus, R., Myhre, C.L., Pfaffhuber, K.A., Wängberg, I., Kyllönen, K., Worthy, D., Martin, L.G., Labuschagne, C., Mkololo, T., Ramonet, M., Magand, O., Dommergue, A. (2018) A vegetation control on seasonal variations in global atmospheric mercury concentrations. *Nature Geoscience* 11, 244–250. https://doi.org/10.1038/s41561-018-0078-8

Jiskra, M., Heimbürger-Boavida, L.E., Desgranges, M.M., Petrova, M.V., Dufour, A., Ferreira-Araujo, B., Masbou, J., Chmeleff, J., Thyssen, M., Point, D., Sonke, J.E. (2021) Mercury stable isotopes constrain atmospheric sources to the ocean. *Nature* 597, 678–682. https://doi.org/10.1038/s41586-021-03859-8

Lamborg, C.H., Hammerschmidt, C.R., Bowman, K.L. (2016) An examination of the role of particles in oceanic mercury cycling. *Philosophical Transactions of the Royal Society A: Mathematical, Physical and Engineering Sciences* 374, 20150297. https://doi.org/10.1098/rsta.2015.0297

Li, C., Jiskra, M., Nilsson, M.B., Osterwalder, S., Zhu, W., Mauquoy, D., Skyllberg, U., Enrico, M., Peng, H., Song, Y., Björn, E., Bishop, K. (2023) Mercury deposition and redox transformation processes in peatland constrained by mercury stable isotopes. *Nature Communications* 14, 7389. https://doi.org/10.1038/s41467-023-43164-8

Luo, Y. (2007) Terrestrial carbon-cycle feedback to climate warming. *Annual Review of Ecology, Evolution, and Systematics* 38, 683–712. https://doi.org/10.1146/annurev.ecolsys.38.091206.095808

Maeda, L., Kawahata, H., Nohara, M. (2002) Fluctuation of biogenic and abiogenic sedimentation on the Shatsky Rise in the western North Pacific during the late Quaternary. *Marine Geology* 189, 197–214. https://doi.org/10.1016/S0025-3227(02)00405-X

Prentice, I.C., Harrison, S.P., Bartlein, P.J. (2011) Global vegetation and terrestrial carbon cycle changes after the last ice age. *New Phytologist* 189, 988–998. https://doi.org/10.1111/j.1469-8137.2010.03620.x

Qu, Y., Zhong, H., Liu, X., Zhang, W., Chen, T. (2024) Coupling and Decoupling Between Sedimentary Mercury and Organic Carbon Preservation in the Oxygenated Marine Environment. *Geochemistry, Geophysics, Geosystems* 25, e2023GC011201. https://doi.org/10.1029/2023GC011201

Rae, J.W.B., Gray, W.R., Wills, R.C.J., Eisenman, I., Fitzhugh, B., Fotheringham, M., Littley, E.F.M., Rafter, P.A., Rees-Owen, R., Ridgwell, A., Taylor, B., Burke, A. (2020) Overturning circulation, nutrient limitation, and warming in the Glacial North Pacific. *Science Advances* 6, eabd1654. https://doi.org/10.1126/sciadv.abd1654

Schmitt, J., Schneider, R., Elsig, J., Leuenberger, D., Lourantou, A., Chappellaz, J., Köhler, P., Joos, F., Stocker, T.F., Leuenberger, M., Fischer, H. (2012) Carbon Isotope Constraints on the Deglacial CO_2 Rise from Ice Cores. *Science* 336, 711–714. https://doi.org/10.1126/science.1217161

Wang, X., Yuan, W., Lin, C.-J., Feng, X. (2022) Mercury cycling and isotopic fractionation in global forests. *Critical Reviews in Environmental Science and Technology* 52, 3763–3786. https://doi.org/10.1080/10643389.2021.1961505

Watson, J.E.M., Evans, T., Venter, O., Williams, B., Tulloch, A., Stewart, C., Thompson, I., Ray, J.C., Murray, K., Salazar, A., McAlpine, C., Potapov, P., Walston, J., Robinson, J.G., Painter, M., Wilkie, D., Filardi, C., Laurance, W.F., Houghton, R.A., Maxwell, S., Grantham, H., Samper, C., Wang, S., Laestadius, L., Runting, R.K., Silva-Chávez, G.A., Ervin, J., Lindenmayer, D. (2018) The exceptional value of intact forest ecosystems. *Nature Ecology & Evolution* 2, 599–610. https://doi.org/10.1038/s41559-018-0490-x

Yokoyama, Y., Esat, T.M., Thompson, W.G., Thomas, A.L., Webster, J.M., Miyairi, Y., Sawada, C., Aze, T., Matsuzaki, H., Okuno, J., Fallon, S., Braga, J., Humblet, M., Iryu, Y., Potts, D.C., Fujita, K., Suzuki, A., Kan, H. (2018) Rapid glaciation and a two-step sea level plunge into the Last Glacial Maximum. *Nature* 559, 603–607. https://doi.org/10.1038/s41586-018-0335-4

Zhang, Y., Jaeglé, L., Thompson, L. (2014) Natural biogeochemical cycle of mercury in a global three-dimensional ocean tracer model. *Global Biogeochemical Cycles* 28, 553–570. https://doi.org/10.1002/2014GB004814